Journal of Alloys and Compounds 509 (2011) 8657–8663

Contents lists available at ScienceDirect

Journal of Alloys and Compounds

journal homepage: www.elsevier.com/locate/jallcom

Nanoindentation characteristics of $Zr_{69.5}Al_{7.5-x}Ga_xCu_{12}Ni_{11}$ glasses and their nanocomposites

Devinder Singh [a], R.K. Mandal [b,*], R.S. Tiwari [a], O.N. Srivastava [a]

[a] Department of Physics, Nano-Science and Technology Unit, Banaras Hindu University, Varanasi 221005, India
[b] Department of Metallurgical Engineering, Nano-Science and Technology Unit, Institute of Technology, Banaras Hindu University, Varanasi 221005, India

ARTICLE INFO

Article history:
Received 7 May 2011
Accepted 16 June 2011
Available online 23 June 2011

Keywords:
Metallic glasses
Quasicrystals
Rapid solidification
Quenching
Mechanical properties
Atomic force microscopy (AFM)

ABSTRACT

This work deals with the indentation behavior of $Zr_{69.5}Al_{7.5-x}Ga_xCu_{12}Ni_{11}$ (x = 0, 1.5, 7.5 at.%) alloys. A comparison between their nanohardness and reduced elastic modulus values of the as-synthesized glassy phase with their nanocomposites has been made. The indentation characteristics of a novel Ga substituted glass composition corresponding to x = 7.5 have shown significant improvement in regard to hardness and elastic modulus. The evidence of pile up has been observed in case of as-synthesized glassy ribbons. The load (P) versus depth (h) curves for as-synthesized melt–spun ribbons displayed the presence of displacement burst, which are known as pop-ins. The amount of energy per unit volume required for the shear band formation in glassy state has been estimated based on the pop-ins observed in P–h curve. This seems to decrease with Ga addition. Based on transmission electron microscopic observations of indented glassy specimen, the possibility of nanocrystallization has been ruled out.

1. Introduction

We report indentation behavior of metallic glass (MG) and glass–nanocrystal (nc)/nanoquasicrystal (nqc) composites in the alloy system $Zr_{69.5}Al_{7.5-x}Ga_xCu_{12}Ni_{11}$ (x = 0, 1.5 and 7.5 at.%). The bulk metallic glass (BMG) composition $Zr_{69.5}Al_{7.5}Cu_{12}Ni_{11}$ (for x = 0) is a widely studied system [1–4]. Various aspects of such BMG like glass forming ability, mechanical behavior, and alloying additions have been investigated. Many alloying additions in this class of BMG have been reported [5–7]. However, Ga addition on Al site has not been studied prior to our detailed investigations on the synthesis and characterization of Ga substituted Zr-based alloy [8]. The alloy design principle adopted in arriving at Ga substituted glass compositions pertains to retaining e/a constant. In this respect, Ga substitution on Al site seems to be ideal. It is well known that Ga is normally substituted in isovalent state vis-a-vis that of Al [9,10]. It is worth-mentioning here that Ga may possess monovalent state. The radius of Ga^{1+} is greater than that of Ga^{3+}. The radius of Ga^{3+} is comparable to Al^{3+}. The mixed valence states of Ga in the glass composition may change the nature of local cluster in the liquid state and there by influencing the crystallization kinetics while annealing the glass at appropriate transformation temperature. The proposition of existence of clusters in supercooled liquid has been in the centre of model of structure of metallic glasses [11]. We refer the readers to our earlier work [8] for knowing nature of crystallization with respect to x. We have also reported changed transformation behavior of glasses at x > 1.5. For x = 0, we have the well investigated Zr-based alloy [1–4] and for x = 7.5, we have a new glass composition. It has been found in earlier studies that minor alloying addition in Zr/Ti-based alloys influences their mechanical, thermal and hydrogen storage properties [12–16]. The purpose of this communication is to compare the indentation behaviors of three glasses (x = 0, 1.5 and 7.5) and their respective nanocomposites obtained after controlled crystallization. We have chosen these for aforesaid reasons. The observation of nanocrystallization during indentation experiment [17–19] is another important area of investigation. We have tried to delineate this with the help of transmission electron microscopic studies on the indented specimen of the as-synthesized glasses. The indentation size effects during micro-/nano-indentations have been reviewed earlier [20]. The studies of mechanical behavior of nanostructured and glassy materials have offered new challenges both from theoretical and experimental aspects. The latter is due to the non-availability of larger size of specimens to conduct tensile, compression or torsion tests [21,22]. Former relates to absence of dislocation activities. Glasses do not have dislocations owing to absence of long range atomic orders where as nano-sized crystalline grains cannot have enough dislocations for plastic deformation. The glass–nqc/nc composites offer new range of complexity of hetero-phase interfaces

* Corresponding author. Tel.: +91 5422369436; fax: +91 5422369478.
E-mail addresses: rkmandal.met@itbhu.ac.in, rkmandal21@yahoo.com (R.K. Mandal).

0925-8388/$ – see front matter © 2011 Elsevier B.V. All rights reserved.
doi:10.1016/j.jallcom.2011.06.076

between the glasses and nqc/nc. Many comprehensive reviews are available in literature on some of these aspects [23,24]. However, the submicroscopic stimulus giving rise to typical signatures during indentation has not been understood so far.

2. Experimental details

The alloy ingots of compositions $Zr_{69.5}Al_{7.5-x}Ga_xCu_{12}Ni_{11}$ (x = 0, 1.5 and 7.5 at.%) were prepared in Ar atmosphere by melting high purity Zr (99.9%), Al (99.96%), Ga (99.99%), Cu (99.99%) and Ni (99.99%) in a silica crucible using a RF induction furnace. The alloys were then melt–spun onto a Cu-wheel rotating at a speed of 40 m/s. The ribbons were prepared by flowing Ar gas continuously. The length and thickness of the ribbons were ~2 m and ~40 μm, respectively. Ribbons thus produced were then packed in a Ta foil and were sealed in a silica ampoule under an Ar atmosphere for annealing experiment.

The as-synthesized ribbons were examined using X-ray diffraction (XRD) and transmission electron microscopy (TEM) to confirm the formation of amorphous phase. The details of structural, microstructural and thermal characterization of as-synthesized as well as those of annealed ribbons have been reported elsewhere [8]. The SHIMADZU HMT-2T microhardness tester was utilized for micro-hardness studies having Vickers indenter. The experiments of nano-indentation were carried out using Hysitron Triboscope 4 with a Berkovich indenter for the as-synthesized as well as heat treated samples. Nano-indentation tests were performed when the thermal drift dropped down to 0.01 nm/s. The impression of indent after the test was examined with the help of Veeco Scanning Probe Microscope having NanoScope IV controller. The indented samples were also observed under environmental scanning electron microscope (ESEM) (Quanta-200) for topological characterization for getting better depth of field. For deciphering the possibility of nanocrystallization, transmission electron microscopic examinations of the indented glassy specimens were carried out. The thinning of such specimen was done from the opposite face of indented surface only. An electron probe micro analysis (EPMA; model: SX100, Ms Cameca, France) was employed for the compositional analysis.

3. Results and discussion

3.1. Microstructural and structural features

We begin this section by giving the TEM micrograph of melt spun ribbon corresponding to $Zr_{69.5}Al_{7.5-x}Ga_xCu_{12}Ni_{11}$ (x = 7.5). As mentioned earlier, this is our novel glass composition and contrast free microstructure is seen in Fig. 1. For x = 0 and x = 1.5, we have observed similar features. The glass–nc/nqc composites are produced after controlled crystallization of melt spun ribbons corresponding to compositions x = 0, x = 1.5 and x = 7.5 [8,25]. For the sake of completeness, we display the TEM micrograph of these composites. Inset in them demonstrate the presence of crystalline/quasicrystalline particles embedded in the glassy matrix (cf. Fig. 2(a–c)). The composition x = 1.5 is the threshold after which the composites consist of two phases embedded in the glassy matrix. These two phases are the icosahedral and Zr_2Cu intermetallic ones. In the Ga bearing glass composition (x = 7.5), we have observed the finer grains of both these phases. We have noted a systematic change in the size of quasicrystalline grain with respect to Ga substitution [8]. We may understand this by recalling expression [26,27] of the steady state nucleation rate (I^s) and is reproduced below

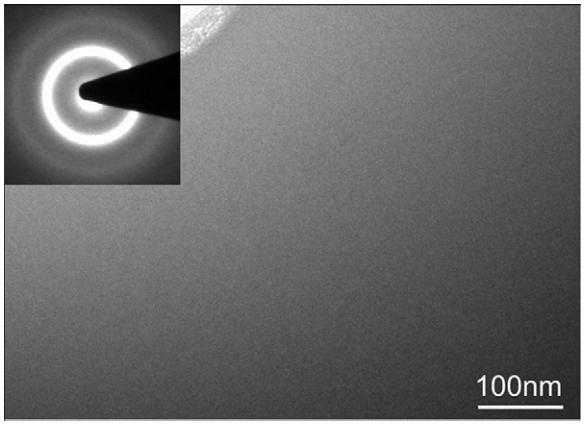

Fig. 1. TEM image and the corresponding diffraction pattern of as-synthesized $Zr_{69.5}Ga_{7.5}Cu_{12}Ni_{11}$ alloy.

$$I^s = A \exp\left[\frac{-16\Pi\sigma^3}{3KT(\Delta G_v)^2}\right] \quad (1)$$

where A = dynamical prefactor, is a function of the atomic mobility at the interface between the nuclei and the liquid/glass and ΔG_v = driving free energy per unit volume for the phase transformation. Within the classical theory of nucleation, the nucleation barrier is governed by interfacial free energy (σ) between the nuclei and the liquid/glass [26]. It indicates that the decrease in σ between the icosahedral quasicrystalline nuclei and the liquid with increasing Ga content contributes to the increase in the nucleation rate. The relevant interfacial energy per unit area of Ga (~0.6 J/m^2) is reported to be lower than that of Al (~1.2 J/m^2) [9,28]. Thus Ga substitution may be reducing the interfacial energy between quasicrystal and remaining amorphous phase, thereby increasing the nucleation rate of the crystalline/quasicrystalline phases. We have evidence of icosahedral phase formation for all the annealed glasses. We therefore surmise that the supercooled liquid has local icosahedral order present predominantly throughout the range of compositions (x = 0–7.5). As a consequence of this we observed icosahedral grains after controlled crystallization of melt spun ribbons (cf. inset of Fig. 2(a–c)). In addition to this, we have formation of Zr_2Cu phase for all compositions above x = 1.5. As mentioned in introduction that Ga may be in 1+ and 3+ states in alloy composi-

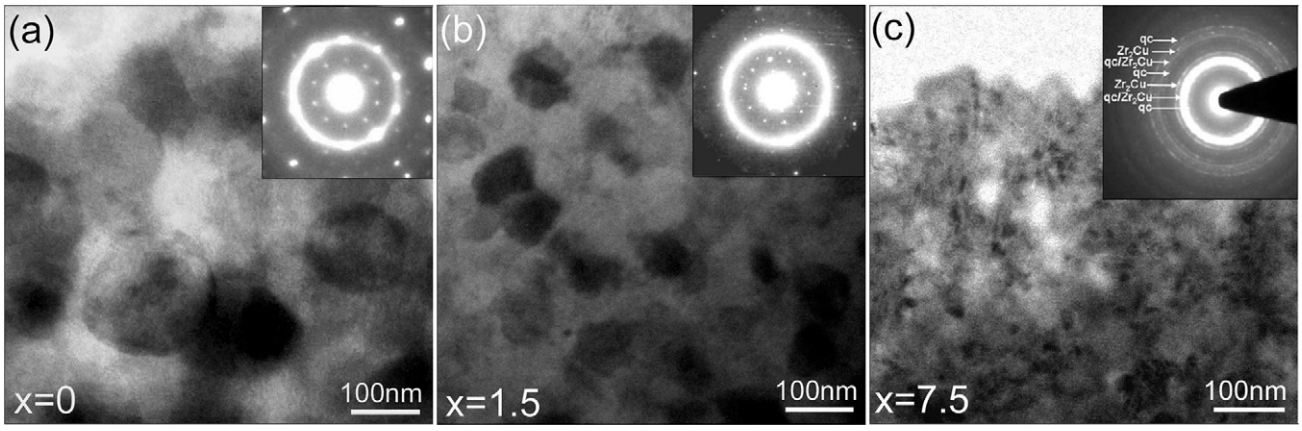

Fig. 2. TEM microstructures and the corresponding diffraction patterns of $Zr_{69.5}Al_{7.5-x}Ga_xCu_{12}Ni_{11}$ alloy with x = 0 (a), x = 1.5 (b) and x = 7.5 (c) formed after heat treatment.

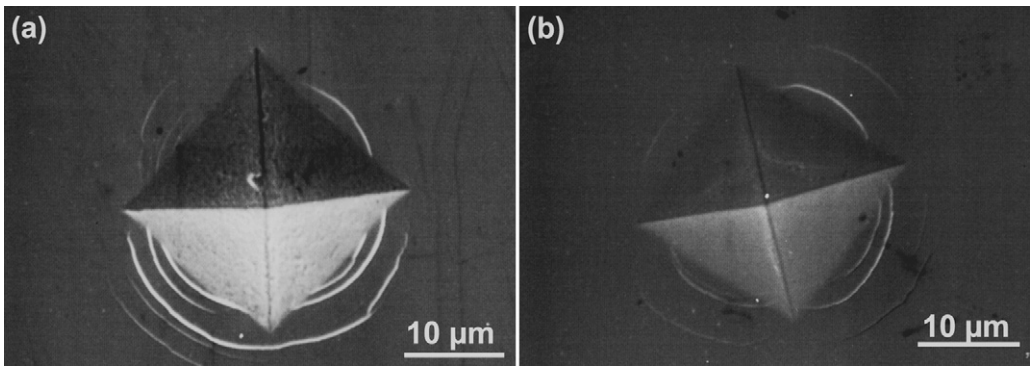

Fig. 3. SEM micrographs for the as-synthesized (a) and annealed ribbons (b) of $x = 7.5$ displaying shear bands.

Table 1
Mechanical properties of as-synthesized and annealed ribbons of $Zr_{69.5}Al_{7.5-x}Ga_xCu_{12}Ni_{11}$ ($x = 0$, 1.5 and 7.5) alloys.

x (at.%)	As-synthesized ribbons			Annealed ribbons		
	Microhardness (GPa) at 100 g load (±0.1)	Nanohardness (GPa) at 5000 μN (±0.2)	Reduced modulus (GPa) at 5000 μN (±5.0)	Microhardness (GPa) at 100 g load (±0.1)	Nanohardness (GPa) at 8000 μN (±0.2)	Reduced Modulus (GPa) at 8000 μN (±5.0)
0	4.7	8.7	98	6.7	11.5	115
1.5	6.1	9.5	112	7.5	12.8	136
7.5	6.6	11.8	140	10.1	14.4	151

tions. The interfacial energy and associated geometrical structure gets influenced by these two electronic states of Ga. Former factor will be responsible in controlling the kinetics of transformation and latter must be changing the associated lattice parameters of the respective phases (icosahedral and Zr_2Cu).

For knowing composition, EPMA was performed for the as-synthesized alloys of $Zr_{69.5}Al_{7.5-x}Ga_xCu_{12}Ni_{11}$ with $x = 0$, 1.5 and 7.5, respectively. Based on the EPMA analysis the composition of the alloys (in at.%) has been found to be $Zr_{69.6}Al_{7.6}Cu_{12.5}Ni_{10.3}$ (for $x = 0$), $Zr_{69.2}Al_{6.2}Ga_{1.6}Cu_{12.8}Ni_{10.2}$ (for $x = 1.5$) and $Zr_{69.4}Ga_{7.7}Cu_{12.5}Ni_{10.4}$

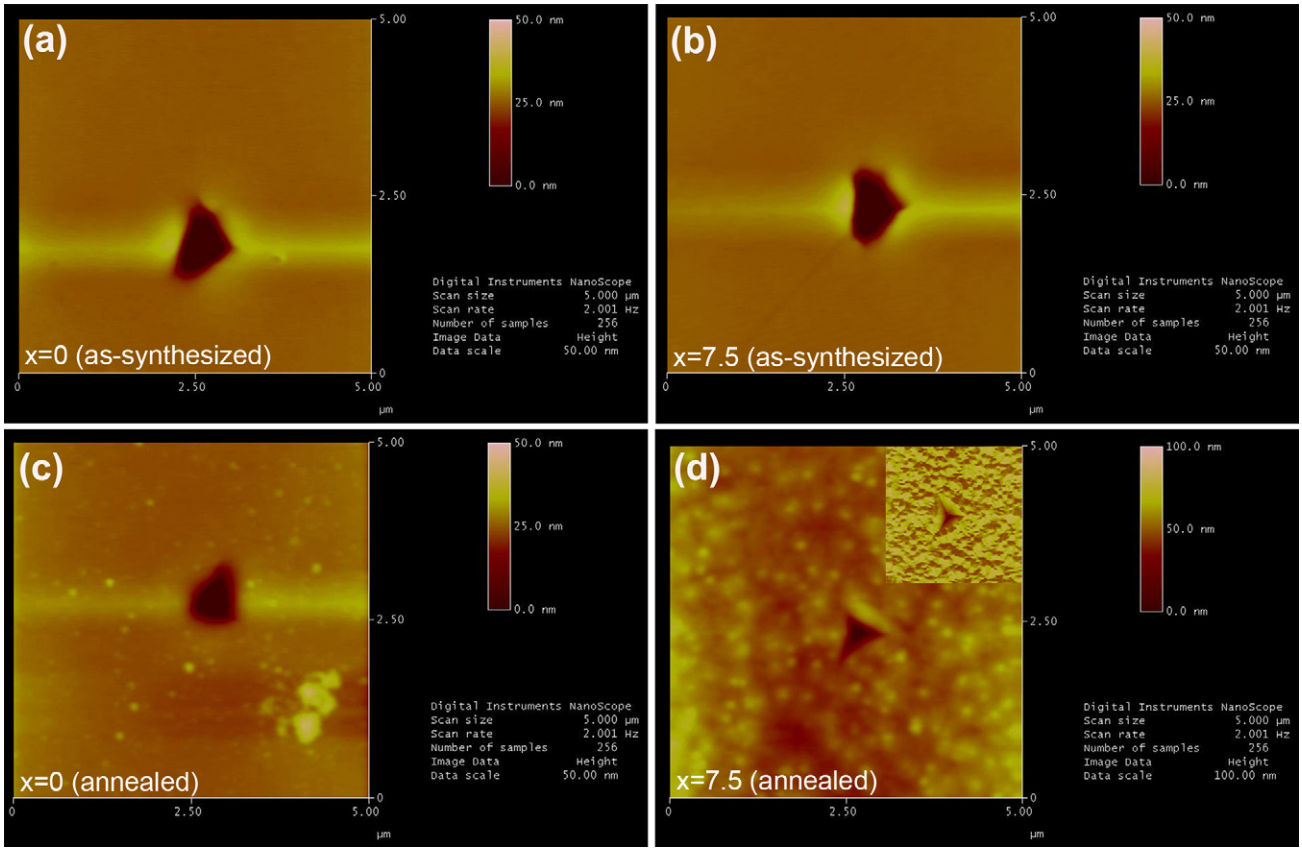

Fig. 4. AFM observation of the nanoindentation imprints from the as-synthesized (a and b) and annealed ribbons (c and d) of $x = 0$ and $x = 7.5$ at 5000 μN. The inset of (d) showing the tip image of nanoindenter.

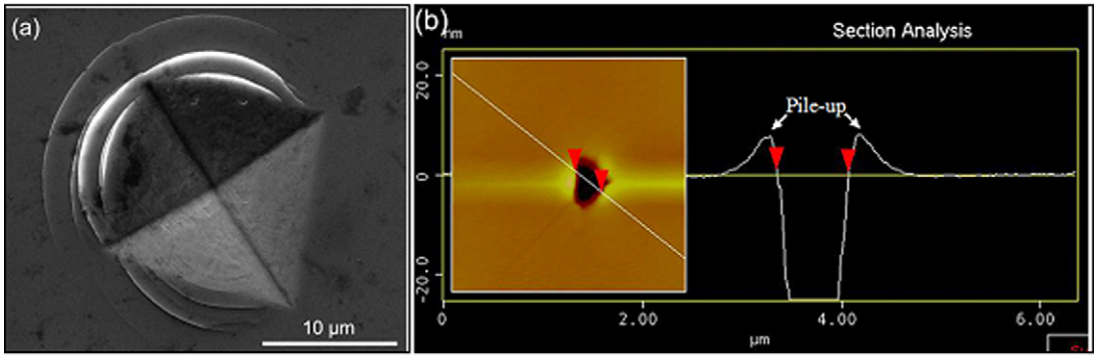

Fig. 5. (a) SEM image of a microindent (Vickers) depicting the formation of shear bands and (b) line scan across nano-indentation (Berkovich) showing the pile-up at its edges for as-synthesized ribbon of $x = 1.5$.

(for $x = 7.5$). Within the limit of detectability of EPMA, no discernible evidence of oxygen in the ribbons was found.

3.2. Indentation behavior

In this section, we present the results of indentation behavior of the three glassy compositions and their respective composites. We have made extensive investigations on the micro-/nano-hardness studies of these materials. Fig. 3 depicts the images of micro-indent for the as-synthesized and annealed ribbons of $x = 7.5$. Table 1 compares the values of microhardness of the glassy as well as their crystallized phases. We have noted a gradual decrease in the number of shear band formation in annealed condition vis-a-vis that of glassy state. After annealing it is the volume fraction of nanocrystalline/nanoquasicrystalline phases, which governs the behavior of indentation. For $x = 7.5$, in addition to quasicrystalline phase, we have Zr_2Cu intermetallics phase also present in the composites. Thus, this glass–nc/nqc composite possesses different indentation characteristics. The presence of nc and nqc must be restricting the propagation of shear band in the glassy matrix during indentation. We note from Table 1 that annealed ribbons for $x = 7.5$ display the highest microhardness value (~10 GPa). This may be the combined effects of decrease in the grain size due to Ga substitution. The value of microhardness at 300 g load for as-synthesized and annealed samples of $x = 1.5$ are ~4.81 GPa and ~5.89 GPa, respectively, which is quite close to that of Zr–Al–Ni–Cu–Ag and Zr–Al–Ni–Cu–Nb metallic glasses and their nanoquasicrystal composites [29].

Having investigated the microhardness behavior of glasses and their composites we now present the results of nanoindentation. This is essential to comprehend the nature of indentation at sub-microscopic scale as well as the plastic deformation under compression of the specimen containing nc/nqc phases in their composites. Fig. 4(a–d) is the indentation impressions of Berkovich indentor at 5000 μN. These are to compare the indentation impressions of the glassy phase with that of their nanocomposite. Fig. 4(a and c) corresponds to $x = 0$, whereas Fig. 4(b and d) refer to $x = 7.5$. The inset in Fig. 4(d) shows the tip image of the nanoindenter. We note clearly the presence of fine grains in Fig. 4(c and d) that are absent in Fig. 4(a and b). The indent size changes with partial crystallization and no cracking occurred. In these images, the height contrast around the impression is due to pile up. The contrast of the pile up in annealed ribbon is not as distinct as it is in case of as-cast glassy sample. The macroscopic flow behavior must be related to shear banding operations. Pile-ups, at which shear band reach the surface, are extensively observed around indents in amorphous alloys [30,31]. The characteristics of the material pile up around the nano-indents were investigated for as-synthesized and annealed ribbons of $x = 1.5$ (Figs. 5 and 6). The formation of shear bands is seen in SEM and AFM images (Fig. 5(a and b)), respectively. The characteristic radial patterns around indentation periphery constitute pile up and an SEM image of micro-indent displays this in Fig. 5(a). The AFM image of the indent and cross sectional profile for the melt spun alloy of $x = 1.5$ are shown in Fig. 5(b). Based on the observations in Fig. 5(a and b) it is clear that the features around the indent represent overlapping layers of displaced material. The plastically displaced material is expected to flow up to the faces of the indenter due to the incompressibility of plastic deformation. This is particularly true in the case of metallic glasses [30]. Fig. 6(a and b) shows the SEM image of a micro-indent and line scan across nanoindentation for annealed ribbon of $x = 1.5$. No significant pile up has been observed in the case of annealed ribbons. Thus, it is evident from Figs. 5 and 6 that the pile up of materials around the indents observed in case of amorphous samples appears to be more significant than that of heat treated samples. The presence of extensive shear bands beneath indents in amorphous alloys has been confirmed by many investigators [32–34].

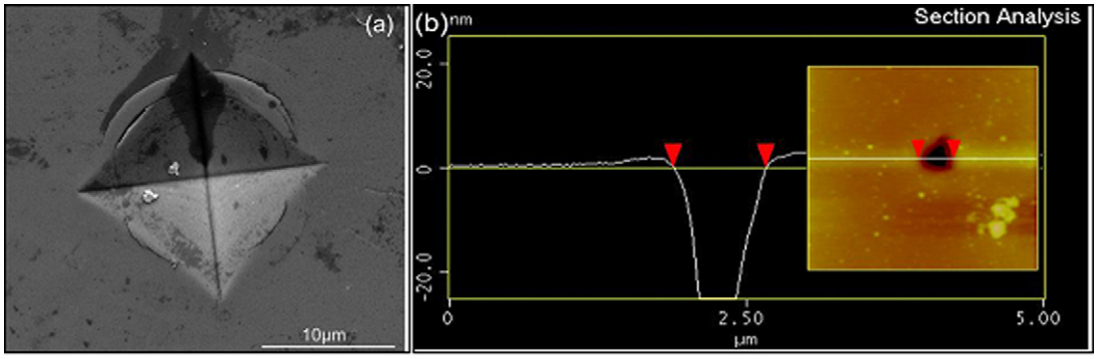

Fig. 6. (a) SEM Image of a microindent (Vickers) and (b) line scan across nano-indentation (Berkovich) for annealed ribbon of $x = 1.5$.

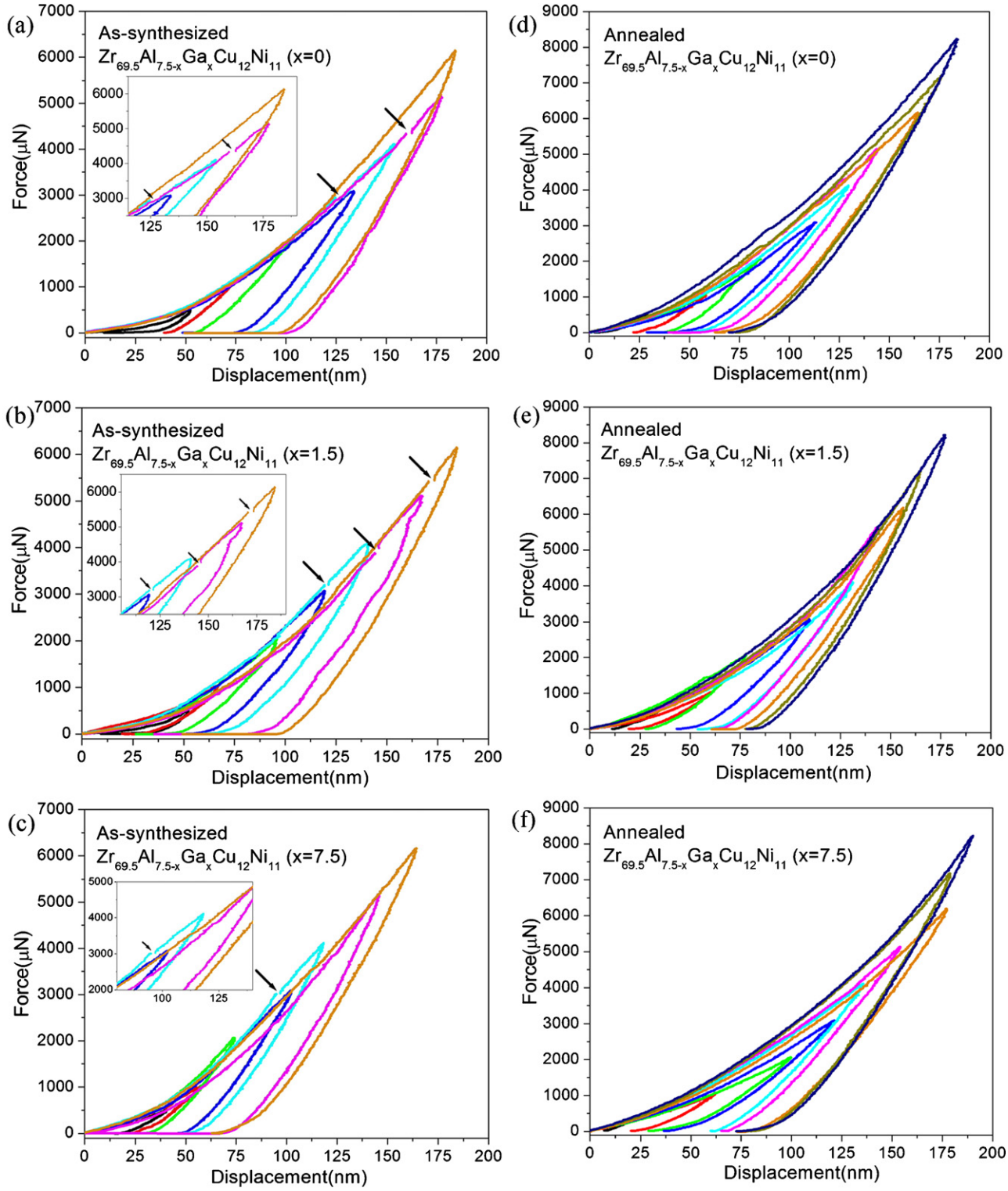

Fig. 7. Plot of the indentation force (P) versus indenter displacement (h) obtained from nanoindentation tests for the as-synthesized (a–c) and annealed (d–f) ribbons of $x = 0$, 1.5 and 7.5, respectively.

Fig. 7(a–c) depict the load (P) versus depth (h) behavior of melt spun ribbons whereas Fig. 7(d–f) displays the P versus h characteristics of their respective composites. Table 1 gives the values of nanohardness and reduced modulus for the alloys with $x = 0$, 1.5 and 7.5, respectively. The nanohardness for the as-synthesized alloys ($x = 0$–7.5) lies in the range ~9–12 GPa. Reduced modulus is one of the fundamental properties and is sensitive to compositions of the alloy as well as atomic arrangements. The reduced modulii for the as-synthesized alloys ($x = 0$–7.5) are found in the range of ~98–140 GPa. Our results of nanohardness and reduced modulus are comparable to those of the Zr-based alloys [24,35,36]. As evident from Table 1, composites possess higher micro-/nanohardness values vis-à-vis those of as-synthesized alloys. Ramamurty et al. [37] reported improvement in stiffness and strength values due

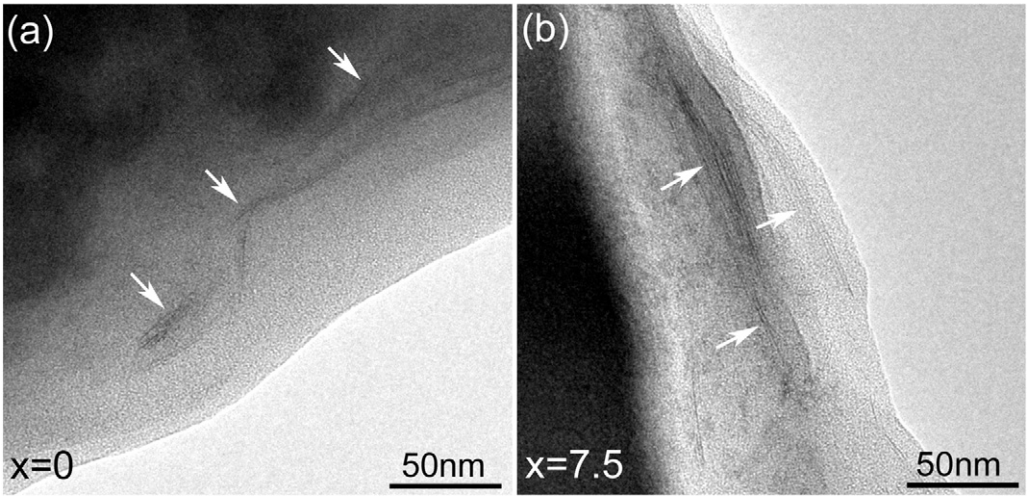

Fig. 8. Bright field TEM images of the indented portion of as-synthesized thinned specimens for $x = 0$ and $x = 7.5$.

to the presence of nanocrystalline particles for the glass–nc composites. As is well known [30,38] mean contact pressure or nanohardness value is higher than that of Vickers hardness value. The difference in the values can be attributed primarily to (i) indentation size effect (ii) actual and projected area of contacts respectively for nano- and micro-hardness measurements. The closer look of P versus h curves (cf. Fig. 7) reveals that for the melt–spun ribbons we have appearance of pop-ins during loading (marked by arrow in Fig. 7(a–c)). According to Drozdz et al. [39], these pop-ins indicating displacement bursts signify the formation of shear bands. They reported prominent pop-ins in case of amorphous alloys while the presence of such events is either less prominent or even completely suppressed in case of annealed alloys. Our observation is in agreement with the results reported earlier [31,39,40]. We do not observe pop-ins in composites. This may be due to the presence of nc/nqc grains in the glassy matrix. The structural features largely dictate the nature of deformation and chemistry can only influence such behavior in a quantitative way. This is the reason why we observe similar kind of P versus h curves corresponding to $x = 0$ and $x = 7.5$ after crystallization of the glasses.

The plastic deformation of metallic glasses during nanoindentation experiment has been found to be typically associated with pop-in events [41,42]. These are associated with the energy barriers for shear band nucleation. The low energy barrier is expected to lead to the easy nucleation of shear bands [42]. By the employment of depth sensitive nanoindentation, the work per unit volume (W/V) required for the formation of shear band induced pop-in burst during nanoindentation loading can be calculated. We have made an attempt to compute the value of W/V during pop-in events of the melt–spun glasses. To accomplish this, we have found out the maximum load (P) and its corresponding value of plastic depth (h_c) at different loads for $x = 0$ and 7.5 specimens. Following this, a linear fit between them was generated. The resulting two equations thus obtained are given by:

$$P_{(x=0)} = 51h_c - 1617 \quad (2)$$

$$P_{(x=7.5)} = 62h_c - 2370 \quad (3)$$

Eqs. (2) and (3), respectively, correspond to MGs with $x = 0$ and $x = 7.5$. For a maximum load of 4000 μN, the loads (F) during pop-in events for $x = 0$ and $x = 7.5$ have been found to be equal to ~2949 μN and ~3015 μN, respectively. Substituting the values of these loads in Eqs. (2) and (3), the corresponding values of plastic displacements are calculated. The amount of energy per unit volume (W/V) required for the pop-in event has been computed by employing following expression:

$$(W/V)_{x=0} = \frac{Fx\Delta d}{Axh_c} \quad (4)$$

where F is the applied force at the pop-in, Δd is the sudden displacement of the indenter during pop-in event; A is the effective area corresponding to the plastic depth h_c. This is obtained with the help of well known relationship $A \approx 24.5\ h_c^2$. Energy per unit volume comes out to be $(W/V)_{x=0} \sim 27 \times 10^{-4}$ eV/Å^3. Following similar procedure and employing Eq. (4) we have got $(W/V)_{x=7.5} \sim 14 \times 10^{-4}$ eV/Å^3. We attribute these energies to be associated with the shear band formation ability of metallic glasses. The energy required for the shear band formation is reduced due to Ga addition. The reduction in energy with Ga addition may be attributed to the good plastic deformation ability and thus good ductility of $Zr_{69.5}Ga_{7.5}Cu_{12}Ni_{11}$ alloy. The observation of pop-ins during loading cannot be attributed to the process of nanocrystallization as noted in reference [43]. The break in the P versus h curves for such a case should appear while unloading. To settle this issue experimentally we have made TEM investigations of the indented portion of these specimens. Fig. 8(a and b) display the bright field images of the as-synthesized thinned specimens for $x = 0$ and $x = 7.5$. These were prepared by masking the indented side and process of thinning was attempted from the opposite side. The bright field images do not show any regions of residual contrast and they resemble analogous to those shown in Fig. 1. We do have evidence of layer wise displacement separated by boundary that is seen as a curvilinear line (marked by arrows). The observation of such lines must be due to the shear band. Thus our experiment rules out the possibility of nanocrystallization.

We now try to explain the change in the mechanical behavior of metallic glasses and their composites on the basis of free volume model. We begin discussion on glasses first. In metallic glass, the free volume exerts a crucial influence on the mechanical properties of amorphous materials, such as hardness, strength and plasticity [44]. In the present case, the increase in the hardness of the metallic glasses may be attributed to the variation of free volume with Ga substitution. Since the atomic radius of Ga (0.141 nm) is intermediate between the atomic radius of Zr (0.160 nm) and Cu (0.128 nm) and the atomic radius of Al (0.143 nm) and Ni (0.125 nm), the Ga substitution may increase the packing density of the alloy [45] and thus would lead to the decrease in the free volume. A low free

volume leads to a high resistance to plastic deformation under applied stress [46]. Such an observation pertaining to the increase in the hardness of metallic glasses with alloying addition has been reported recently [45]. The primary carriers of plasticity in amorphous materials are the shear transformation zones (STZs) [23,47]. The availability of free volume is critical for the STZs to occur. In the case of glass–nc/nqc composites, the free volume decreases due to the precipitation of the nc/nqc phases and this causes densification of the metallic glass [48]. This process makes the operation of STZs difficult which results in an increased resistance to plastic deformation and therefore enhancement of hardness of the metallic glass upon structural relaxation and nanocrystallization. This effect is consistent with the results reported earlier [49,50]. Further, increase in the hardness of the glass-nc/nqc composites with increase in the addition of Ga concentration may be due to the grain refinement of nanocrystals/nanoquasicrystals, which produces many interfaces leading to the strengthening phenomenon.

4. Conclusions

We have compared the nanoindentation behaviors of $Zr_{69.5}Al_{7.5-x}Ga_xCu_{12}Ni_{11}$ ($x = 0$, 1.5 and 7.5 at.%) glasses with their composites. The effect of Ga substitution on the nature of indentation and reduced elastic modulus has been reported. It has been found that the indents observed in case of amorphous samples exhibit a relatively larger amount of pile-up than those of annealed samples. The pop-ins was observed only in the case of as-synthesized melt spun ribbons. The energy per unit volume required for the shear band formation in the glass has been estimated with the help of P–h curve. This seems to decrease with addition of Ga. Based on transmission electron microscopic studies of the indented glassy specimen, the possibility of nanocrystallization has been ruled out.

Acknowledgements

The authors are thankful to Prof. N.K. Mukhopadhyay, Dr. M.A. Shaz and Dr. T.P. Yadav for many stimulating discussions. We acknowledge the technical helps received in conducting TEM/SEM and AFM/Nanoindentation studies, respectively, by Mr. Vijay Kumar and Mr. Manjeet Singh. Financial assistance received from Department of Science and Technology (UNANST, DST) is gratefully acknowledged. One of us (Devinder Singh) thanks Council of Scientific and Industrial Research (CSIR), New Delhi for the award of a Senior Research Fellowship.

References

[1] U. Koster, J. Meinhardt, S. Roos, H. Liebertz, Appl. Phys. Lett. 69 (1996) 179–181.
[2] A. Inoue, Acta Mater. 48 (2000) 279–306.
[3] W.H. Wang, C. Dong, C.H. Shek, Mater. Sci. Eng. R 44 (2004) 45–89.
[4] A. Inoue, T. Zhang, M.W. Chen, T. Sakurai, J. Saida, E. Matsubara, Appl. Phys. Lett. 76 (2000) 967–969.
[5] J. Saida, M. Matsushita, C. Li, Appl. Phys. Lett. 76 (2000) 3558–3560.
[6] C.T. Liu, Z.P. Lu, Intermetallics 13 (2005) 415–418.
[7] C. Fan, H. Choo, P.K. Liaw, Scripta Mater. 53 (2005) 1407–1410.
[8] D. Singh, T.P. Yadav, R.K. Mandal, R.S. Tiwari, O.N. Srivastava, Mater. Sci. Eng. A 527 (2010) 469–473.
[9] M. Heinzig, C.J. Jenks, M.V. Hove, I. Fisher, P. Canfield, P.A. Thiel, J. Alloys Compd. 338 (2002) 248–252.
[10] D. Singh, T.P. Yadav, R.S. Tiwari, O.N. Srivastava, J. Mater. Sci. 44 (2009) 3883–3888.
[11] K.F. Kelton, G.W. Lee, A.K. Gangopadhyay, R.W. Hyers, T.J. Rathz, J.R. Rogers, M.B. Robinson, D.S. Robinson, Phys. Rev. Lett. 90 (2003) 195504–195514.
[12] M. Iqbal, W.S. Sun, H.F. Zhang, J.I. Akhter, Z.Q. Hu, Mater. Sci. Eng. A 447 (2007) 167–173.
[13] S. Nowak, P. Ochin, A. Pasko, O. Maciejak, P. Aubert, Y. Champion, J. Alloys Compd. 483 (2009) 139–142.
[14] D. Singh, T.P. Yadav, R.K. Mandal, R.S. Tiwari, O.N. Srivastava, Phil. Mag. 91 (2011) 2837–2845.
[15] T. Burgess, M. Ferry, Mater. Today 12 (2009) 24–32.
[16] R.R. Shahi, T.P. Yadav, M.A. Shaz, O.N. Srivastava, S.V. Smaalen, Int. J. Hydrogen Energy 36 (2011) 592–599.
[17] A. Inoue, W. Zhang, T. Tsurui, A.R. Yavari, A.L. Greer, Phil. Mag. Lett. 85 (2005) 221–237.
[18] J.J. Lewandowski, A.L. Greer, Nat. Mater. 5 (2006) 15–18.
[19] J. Fornell, E. Rossinyol, S. Surinach, M.D. Baro, W.H. Li, J. Sort, Scripta Mater. 62 (2010) 13–16.
[20] N.K. Mukhopadhyay, P. Paufler, Int. Mater. Rev. 51 (2006) 209–245.
[21] K.S. Kumar, H.V. Swygenhoven, S. Suresh, Acta Mater. 51 (2003) 5743–5774.
[22] U. Ramamurty, S. Jana, Y. Kawamura, K. Chattopadhyay, Acta Mater. 53 (2005) 705–717.
[23] C.A. Schuh, T.C. Hufnagel, U. Ramamurty, Acta Mater. 55 (2007) 4067–4109.
[24] M.M. Trexler, N.N. Thadhani, Prog. Mater. Sci. 55 (2010) 759–839.
[25] D. Singh, T.P. Yadav, R.K. Mandal, R.S. Tiwari, O.N. Srivastava, Intermetallics 18 (2010) 2445–2452.
[26] K.F. Kelton, J. Non-Cryst. Solids 334–335 (2004) 253–258.
[27] J.N. Mei, J.S. Li, H.C. Kon, H.Z. Fu, L. Zhou, J. Non-Cryst. Solids 354 (2008) 3332–3335.
[28] T.P. Yadav, M.A. Shaz, R.S. Tiwari, O.N. Srivastava, Formation and stability of icosahedral phase in $Al_{65}Ga_5Pd_{17}Mn_{13}$ alloy, Phil. Mag. 88 (2008) 1995.
[29] J.B. Qiang, W. Zhang, G. Xie, H. Kimura, C. Dong, A. Inoue, Intermetallics 15 (2007) 1197–1201.
[30] R. Vaidyanathan, M. Dao, G. Ravichandran, S. Suresh, Acta Mater. 49 (2001) 3781–3789.
[31] J.J. Kim, Y. Cho, S.A. Suresh, S. Argon, Science 295 (2002) 654–657.
[32] S. Jana, U. Ramamurty, K. Chattopadhyay, Y. Kawamura, Mater. Sci. Eng. A 375–377 (2004) 1191.
[33] Y.F. Shi, M.L. Falk, Appl. Phys. Lett. 86 (2005) 011914.
[34] L. Anand, C. Su, Mech. Phys. Solids 53 (2005) 1362.
[35] J.G. Wang, B.W. Choi, T.G. Nieh, C.T. Liu, J. Mater. Res. 15 (2000) 798–807.
[36] N.H. Tariq, B.A. Hasan, J.I. Akhter, F. Ali, J. Alloys Compd. 469 (2009) 179–185.
[37] U. Ramamurty, N. Nagendra, Y. Li, J. Metastruct. Mater. 10 (2001) 61–66.
[38] L. Qian, M. Li, Z. Zhou, H. Yang, X. Shi, Surf. Coat. Technol. 195 (2005) 264–271.
[39] D. Drozdz, T. Kulik, H.J. Fecht, J. Alloys Compd. 441 (2007) 62–65.
[40] S. Azad, A. Mandal, R.K. Mandal, On the parameters of glass formation in metallic systems, Mater. Sci. Eng. A 458 (2007) 348–354.
[41] Mingwei Chen, Ann. Rev. Mater. Res. 38 (2008) 445.
[42] K. Wang, M.W. Chen, D. Pan, T. Fujita, W. Zhang, X.M. Wang, A. Inoue, Mater. Sci. Eng. B 148 (2008) 101.
[43] C. Fischer-Cripps Anthony, in: F. Frederick, Ling (Eds.), Nano-Indentation, Mechanical Engineering Series, Springer-Verlag, New York, LLC, 2004.
[44] L.Y. Chen, Z.D. Fu, G.Q. Zhang, X.P. Hao, Q.K. Jiang, X.D. Wang, Q.P. Cao, H. Franz, Y.G. Liu, H.S. Xie, S.L. Zhang, B.Y. Wang, Y.W. Zeng, J.Z. Jiang, Phys. Rev. Lett. 100 (2008) 075501–075504.
[45] J.S.C. Jang, S.R. Jian, C.F. Chang, L.J. Chang, Y.C. Huang, T.H. Li, J.C. Huang, C.T. Liu, J. Alloys Compd. 478 (2009) 215–219.
[46] W.H. Jiang, F.E. Pinkerton, M. Atzmon, Acta Mater. 53 (2005) 3469–3477.
[47] A. Dubach, F.H. Dalla Torre, J.F. Loffler, Acta Mater. 57 (2009) 881–892.
[48] D.I. Uhhenhaut, F.H. Dalla Torre, A. Castellero, C.A.P. Gomez, N. Djowrelon, G. Krauss, B. Schmitt, B. Patterson, J.F. Loffler, Phil. Mag. 89 (2009) 233–248.
[49] S. Xie, E.P. George, Acta Mater. 56 (2008) 5202–5213.
[50] B.G. Yoo, K.W. Park, J.C. Lee, U. Ramamurty, J.I. Jang, J. Mater. Res. 24 (2009) 1405–1416.